ISSN No:-2456-2165 https://doi.org/10.38124/ijisrt/25apr652

Data Evaluation and Modeling of Billet Characteristics in the Steel Industry

Maaz Bahauddin Naveed[1]

[1]AL Qaryan Group

Publication Date: 2025/05/02

Abstract: This study presents a methodology to analyze and model the continuous mill process of billets in steel plants. A reliable billet tracking system able to track each workpiece from the furnace entrance to the exit area of the rolling mill stands is designed based on information derived from rolling mill signals processed through advanced data science algorithms. From the stored information, two issues are solved: the data of the thermal sensors (of a thermographic camera or pyrometers) and the current linked to the absorption of the rolling mill stands; and a mathematical modelisation of the temperature of the billets along its way through the rolling mill is elaborated. Based on this data analysis, we concluded that some hardware changes were needed: the IR camera was moved to eliminate the interference of the scaly formation of the sensor with the data collected. The modelization step served as a foundation for future applications of control and/or diagnosis that will make use of a temperature decay model.

Keywords: *Steel Industry; Reheating Furnace; Rolling Mill Stands; Billet; Tracking System; Data Analysis; Modelization.*

How to Cite: Maaz Bahauddin Naveed (2025). Data Evaluation and Modeling of Billet Characteristics in the Steel Industry. *International Journal of Innovative Science and Research Technology*, 10(4), 2181-2197. https://doi.org/10.38124/ijisrt/25apr652

I. INTRODUCTION

Global Overview of Energy Consumption in the Secondary Sector. The secondary sector globally is a significant consumer of energy, particularly through various energy-intensive processes found in industries such as metallurgy, petrochemicals, textiles, cement, and food production. The implementation of Green Economy energy policies has become increasingly relevant to engineers and researchers; these policies offer essential strategies for managing and reducing environmental risks associated with high-energy consumption processes. This necessitates the design and execution of proactive measures.

In recent years, several initiatives have emerged on both global and national fronts aimed at sustainability. Notably, Agenda 2030 serves as a framework at an international level while Italy's National Recovery Plan (PNRR) addresses similar objectives within its borders. Within metallurgical sectors specifically, steel manufacturing stands out as one of the most critical industries due to its substantial economic significance nationally and internationally. Various stages involved in steel production are characterized by their considerable energy demands—both electrical and thermal—which can be leveraged to minimize CO2 emissions effectively.

Achieving reductions in CO2 emissions presents a challenging yet attainable goal that can be pursued through hardware upgrades or alternative techniques that do not adversely affect plant operations. These approaches often employ data analytics alongside modeling techniques supported by control optimization algorithms.

Energy consumption during furnace reheating processes is crucial for producing quality products within the steel industry. Semi-finished goods like billets undergo heating before being deformed into desired shapes using rolling mill stands; hence specifications vary depending on the final product type produced (e.g., rods or bars). The current study aims to establish methods for analyzing data related to billet processing within rolling mills situated in steel manufacturing facilities.

To enhance energy efficiency without compromising product integrity requires advanced monitoring systems along with optimized controls throughout reheating cycles leading up to rolling phases since real-time temperature tracking for billets currently lacks adequate information sources available today.

Data correlations—linking measurements from live processed billets including triggers from photocells alongside temperature readings—need development despite existing limitations posed by sensor technologies if effective applications concerning monitoring practices are intended. Numerous methodologies pertaining to data analysis specific to modelization efforts employed across different automation levels have been discussed extensively across literature channels regarding this subject matter. For instance:

- A generative adversarial network-based technique proposed augmentation solutions designed around missing multivariate time-series datasets,
- An anomaly detection approach utilizing multi-criteria evaluations tailored explicitly toward handling discrepancies visible via energetic dataset outputs,

ISSN No:-2456-2165 https://doi.org/10.38124/ijisrt/25apr652

Additionally noted was research applying adaptive fuzzy C-means algorithms targeted towards identifying outliers based upon collected metrics analyzed under extensive conditions observed surrounding operational parameters tied directly back into neural networks facilitating further exploration down paths linked towards smart frameworks encapsulated within Industry 4 contexts demonstrating automated identification mechanisms integrated utilizing vision-based modalities directed primarily toward tracking manufactured outcomes derived thereafter linking technological insights drawn forth resulting regression dependencies accounting historical influences impacting overall performance dynamics observed consistently monitored environments over sustained periods documenting throughput variances encountered thereby substantiating findings described herein prior investigative endeavors documented previously elsewhere encompassing multiple aspects integral thus far detailed hereinafter moving forward optimally capturing nuances elucidated therein unveiled prospects awaiting realization ahead!

A predictive structure founded upon gate recurrent units forecasts internal temperatures reliant strictly upon correlational relationships established among fuel inputs together combined airflows measured sequentially captured respectively via temporal snapshots gathered accordingly reflecting transient heat conduction principles laid bare employing finite-difference constructs developed uniquely illustrating underlying mechanics governing heated state transitions occurring systematically witnessed firsthand traversing varying configurations evaluated meticulously conducted shown subsequently addressing gaps recognized presently pervasive shortcomings hindering comprehensive understandings prevailing ultimately underscoring need arising clearly delineated points outlined earlier preceding sections advocating thorough inquiries warranted advancing knowledge base collectively cultivated intensively explored expounded diligently compiling results yielded accompanied discussions presented concluding remarks synthesized succinctly encapsulating main takeaways formulated offering directions guiding future explorations anticipated forthcoming ventures!

II. MATERIALS AND METHODS

A. Process Description

The current document discusses the reheating furnaces and rolling mills found within steel manufacturing facilities. The primary materials undergoing processing in these systems are known as billets (refer to Figure 1). In the facility under consideration, the dimensions of these billets measure either 0.14 m × 0.14 m or 0.16 m × 0.16 m, with lengths ranging from 7 to 12 meters.

Fig 1 Example of a Billet.

This research utilizes a walking beam reheating furnace as an illustrative example of a distinct type of furnace model [11,28]. Billets are introduced into the furnace using designated pushers (front charging), ensuring they remain spaced apart. Their movement within the furnace is regulated by a mechanism that lifts and advances them forward (or backward) in specified increments, which are primarily determined by the cross-section of the billets. In this manner, the billets progress through the furnace until they reach the rolling mill stands, where hot rolling takes place (Figure 2).

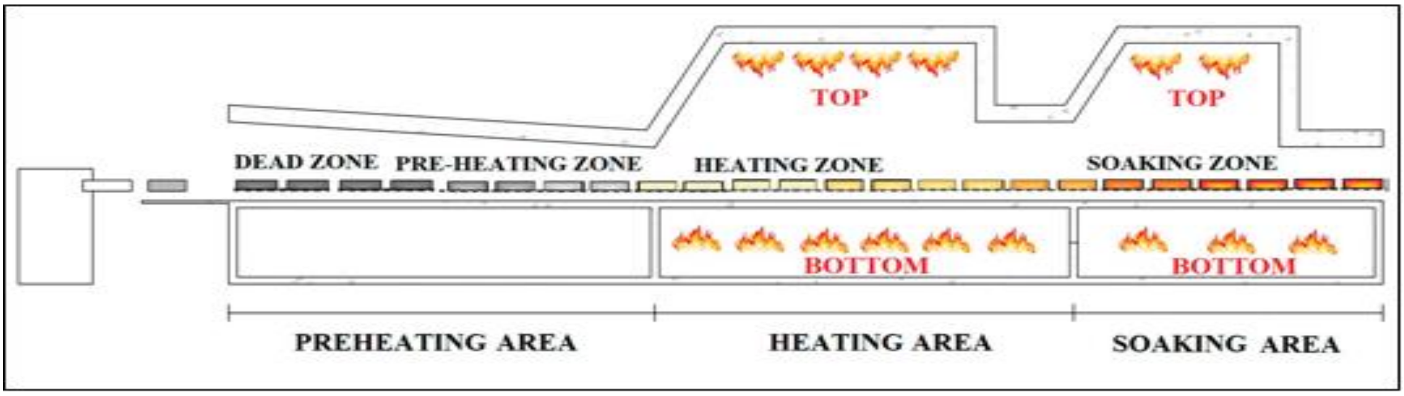

Fig 2 Schematic Representation of the Reheating Furnace.

An optical pyrometer positioned near the entrance of the furnace measures the temperature of the upper surface of billets. The billets processed in this facility are primarily cold, with those entering from Forge typically around 30 °C at the furnace inlet. As depicted in Figure 2, these billets enter on the left side; however, during approximately the first half (Preheating Area), there are no active burners present. This Preheating Area includes a non-active region and a preheating zone devoid of burner activity. A chimney is situated nearby to allow for smoke discharge.

ISSN No:-2456-2165 https://doi.org/10.38124/ijisrt/25apr652

Once they pass through this Preheating stage, billets transition into what is known as Heating Area where critical heating occurs. Following that, they move into Soaking Area—commonly referred to as furnace soaking—which ensures uniformity in their heating prior to leaving the furnace. The equalization phase addresses balancing heat distribution between both ends (head and tail) relative to their arrangement shown in Figure 3. This step is vital within a reheating system since different temperatures may be necessary for each end due to delays experienced during processing at rolling mill stands.

As illustrated by Figure 2, billet temperatures increase throughout their time spent inside the furnace: this reheating process is represented by a color gradient ranging from grey to red in Figure 2 itself—where grey indicates colder billets still undergoing preheating; yellow and orange denote those currently being heated; while red marks segments that have reached soaking conditions. Additionally, because it employs walking beam technology, gaps exist between individual billets which are indicated alongside respective zone lengths detailed in Table 1.

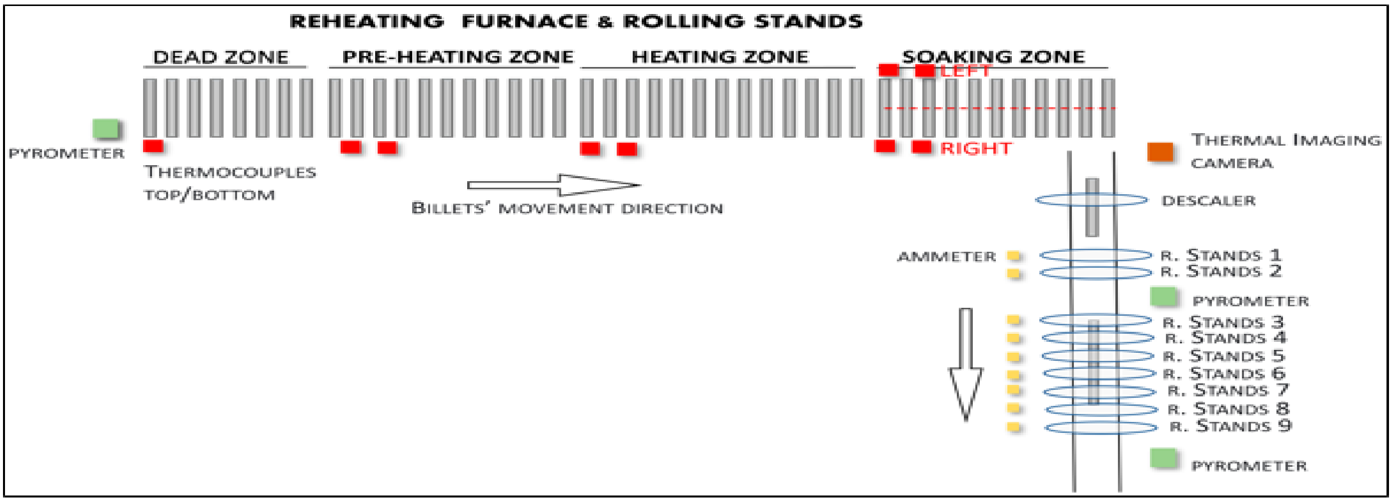

Fig 3 Original Configuration of the Plant.

Table 1 Furnace Zone lengths.

Furnace Zone	Length
Dead Zone	5.4m
Pre-Heating Zone	4.1m
Heating Zone	6.1m
Soaking Zone	3.4m

Within each furnace zone, the temperature (excluding dead zones) is tracked using two thermocouples positioned at both the top and bottom of the zone. The Soaking Area contains two firing zones (left and right), with thermocouples installed in both upper and lower sections of the furnace. Additionally, a thermocouple located in the smoke exchanger monitors temperatures within any dead zones. Active burners are situated in both Heating and Soaking Areas above and below (see Figure 2). The Soaking Area comprises independent burners across its left and right firing areas, as illustrated in Fig. 3.

For every burner along these furnace zones, Proportional-Integral-Derivative (PID) controllers operate under a master-slave configuration; here, top burners function as masters while bottom ones serve as slaves [29]. Specifically, PID setpoints are adjusted based on several factors including production rate from the furnace inlet temperature to material quality for steel products aimed for completion—ensuring an outlet-billet temperature around 1200°C with PID settings ranging between 1080–1230°C.

A more comprehensive layout of both reheating furnaces and rolling mill stands can be found in Fig. 3 which we will refer to as original configuration throughout this discussion. All sensors alongside features outlined previously have been documented within this figure.

As shown there, a thermal camera sensor is established at the exit area when taking into account reference from one side of longitudinal axis through to another end point of that same section; it captures final billet temperatures post-first heating phase before semi-finished goods transition onto rollers leading towards descaler devices designed specifically to eliminate surface scale or impurities arising due oxidation during heat treatment process via high-speed water jets used effectively by said machines .

The presence scales leads problems impacting measurements taken by our thermal sensors since their characteristics typically exhibit lower readings compared against actual semi-finished product values [30][31].After undergoing cleaning measures provided through aforementioned descalers , billets advance toward rolling phases represented visually again inside Figure three ; comprised therein consists essentially outlaying two sub-

ISSN No:-2456-2165 https://doi.org/10.38124/ijisrt/25apr652

phases where initial transport roller paths direct them straightly onward reaching first stages —stands numbered sequentially starting off labelled simply '1' & '2.' Upon arrival here , they undergo necessary straightening actions prior checking accomplished utilizing optical pyrometer assessing current state billeting's respective temps followed closely thereafter navigating onwards further down range engaging additional stands identified distinctly now numerically tallied up reaching total count seven elaborated visibly upon visual aids already present earlier .

This second round then concludes measuring output via yet another optical pyrometer stationed precisely marking endpoint observed overall distance stretching roughly estimated length ~50m separating furthest reaches exiting former confines initially described until hitting last sensing apparatus encountered close proximity whilst movement speed averages remain calculated somewhere nearby approximately just about ~1 m/s . Detailed calibration tests were conducted ensuring reliability data acquisition amongst different instruments listed accordingly Table Two supports verifying accuracy achieved coordination aligning measurement results obtained directly article device implementations such compact style pyrometers employed efficiently throughout entire operations witnessed firsthand collectively enabling precise oversight monitoring undertaken continuously without fail...

Table 2 Thermal Imaging Camera's and Pyrometers Measuring Range.

Sensor	**Measuring Range**
Furnace Inlet Pyrometer	0–500 ˚C Thermal
Imaging Camera	675–1800 ˚C (1 kHz) First
Rolling Mill Pyrometer	700–1200 ˚C
Second Rolling Mill Pyrometer	700–1100 ˚C

After completing the initial characterization phase discussed in this paper, adjustments were made to the field configuration to enhance data reliability from the thermal imaging camera measurements. This was primarily due to concerns regarding the scale present on the surface of the billet (refer to Section 3). The revised configuration is illustrated in Figure 4. A comparison between the original setup (Figure 3) and this modified arrangement reveals a singular alteration: specifically, the relocation of the thermal imaging camera. In its original placement, it was situated at furnace exit; however, in the updated configuration, it has been repositioned after the descaler device and prior to entering the first mill stand in sequence.

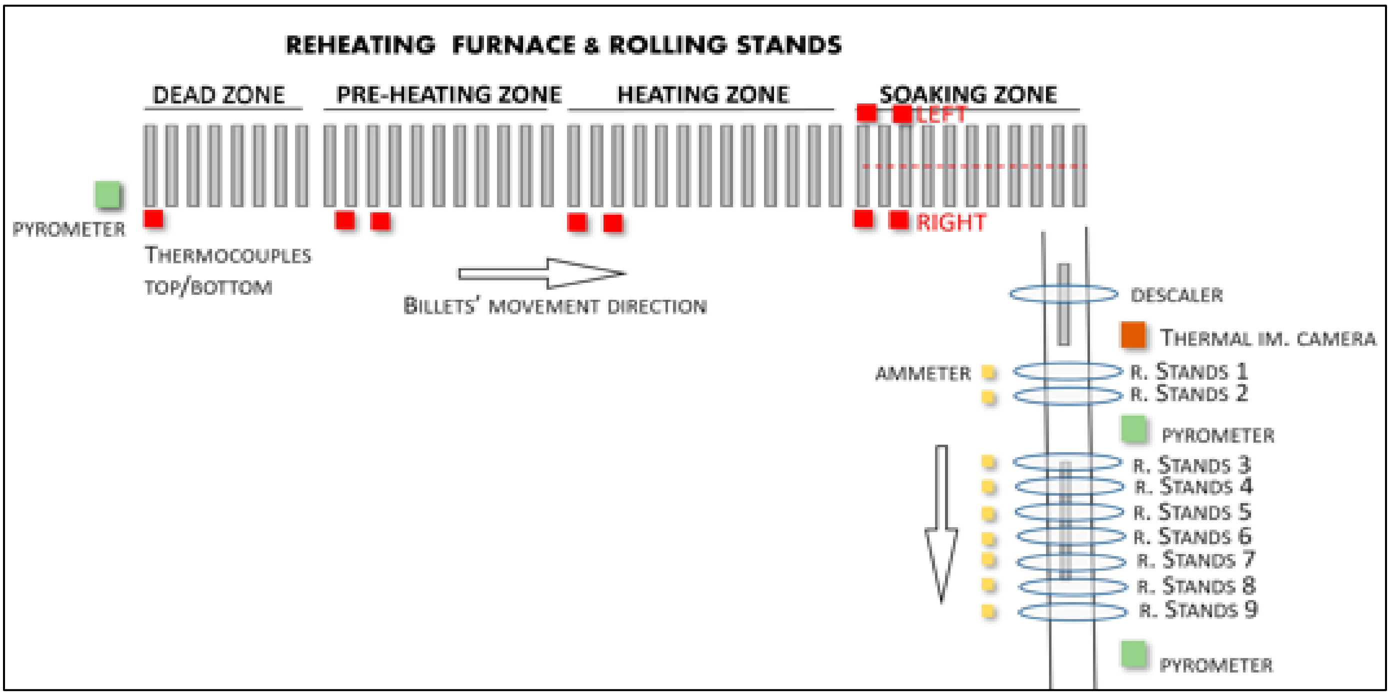

Fig 4 Modified Configuration of the Plant.

B. Data Selection, Acquisition, and Storage

The same procedures for selecting, acquiring, and storing plant data have been implemented. The collection of plant data was conducted in the field using Programmable Logic Controllers (PLCs) [10]. Initially, a careful selection process for the data was performed. Table 3 provides details regarding the billets, reheating furnace, and rolling mill that were used in this research study [1].

ISSN No:-2456-2165 https://doi.org/10.38124/ijisrt/25apr652

Table 3 Data that were selected for the Proposed Study.

Signal	Subprocess
Zones Temperature	Reheating Furnace
Smoke Exchanger Temperature	Reheating Furnace
Furnace Inlet Pyrometer	Reheating Furnace
Furnace Inlet Photocells	Reheating Furnace
Billet Charging Trigger	Reheating Furnace
Iron Wire Tie Counter	Reheating Furnace
Furnace Step Forward Triggers	Reheating Furnace
Furnace Step Backward Triggers	Reheating Furnace
Furnace Step Magnitudes	Reheating Furnace
Furnace Exit Photocell	Reheating Furnace
Billet Discharge Trigger	Reheating Furnace
Billet Re-Charging Trigger	Reheating Furnace Thermal
Billet Re-Charging Trigger	Reheating Furnace/Rolling Mill
Rolling Mill Inlet Photocell	Rolling Mill
Rolling Mill Stands' Triggers	Rolling Mill
Rolling Mill Exit Photocell	Rolling Mill
First Rolling Mill Pyrometer	Rolling Mill
Second Rolling Mill Pyrometer	Rolling Mill
Ambient Temperature	Rolling Mill
Rolling Mill Stands' Absorption	Rolling Mill Billet Geometry

A suitable architecture for the collection and storage of data required for the study has been developed (Figure 5). The selected data were sourced from PLCs within the plant (PLC data—Plant PLCs, Figure 5), as previously outlined. These PLCs manage essential levels of automation; they ensure both operational efficiency and safety within the facility. A PC server located at the plant was integrated into its network infrastructure. This setup includes a PC Server that supports SCADA functions and database management, as depicted in Figure 5 [1,2,10].

The processes related to data selection, acquisition, and storage have been established on this PC server. Additionally, a client workstation has been installed in the control room of the reheating furnace to relay specific signal information to operators and engineers onsite. The design aimed to make presented content user-friendly through customized techniques for data visualization.

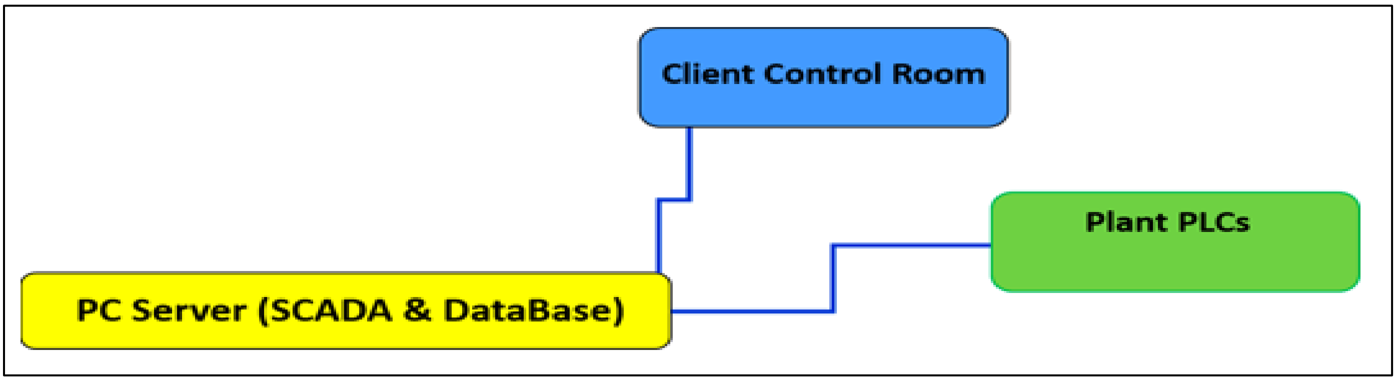

Fig 5 Designed Configuration for data Acquisition and Storage.

C. Billet Tracking System

A billet tracking system has been established to utilize the information stored within a created database. This system takes into consideration the collected data, including plant details and both original and modified configurations (referenced in Figures 3 and 4). It monitors each processed billet from its entry into the reheating furnace until it exits through the rolling mill stands. Typically, data gathered from field sensors may contain acquisition errors or device malfunctions. To address this issue, suitable pre-processing techniques—such as validity thresholds along with checks for spikes and freezes—are employed to identify and eliminate unreliable data. These validity limits, along with spike detection parameters, are calibrated based on sensor specifications as well as historical datasets.

To ensure that outputs from the billet tracking system conform to a specific format, consistent data is utilized throughout its structure; this comprises 15 columns where each row represents one processed billet's "history." The initial column documents various features of the billets—including mass, length, cross-section dimensions per unit length—and their respective reheating groups which dictate target heating curves for those billets. The second column

ISSN No:-2456-2165 https://doi.org/10.38124/ijisrt/25apr652

indicates steel quality codes alongside diameters applicable to final products post-rolling phase of selected billets.

The third column logs timestamps marking when billetes arrive at the furnace entrance while temperatures recorded by an inlet pyrometer corresponding to these arrivals appear in Column four. Column five outlines discretization time steps during which billets were situated within the furnace environment while sixth provides a matrix detailing thermocouple readings related specifically to them according to fifth-column entries.

For measurements concerning rolling mill stands operations replicate similar processes using exit times from furnaces combined with ambient temperature records captured via thermal imaging cameras alongside two designated pyrometers used in conjunction with absorption rates noted for individual stands—all linked back through appropriate discretization timestamps. Additionally, further insights regarding billeting arise through this tracking mechanism—for example: if any given billet was fitted with an iron wire tie requiring removal by operators upon exiting furnaces thus resulting abnormal dwell durations within certain rolling mills' frameworks—or instances whereby relaying back occurred due unplanned events transpiring inside said milling environments.

D. Data Analysis

Data analysis methodologies were utilized based on the outputs generated by the billet tracking system. In particular, correlation and regression techniques were employed [32, 33,[35]. The data provided by this system facilitated the calculation of both the correlation coefficient and determination index between measured temperature values and absorption rates recorded across all stands following each evaluated billet. Additionally, graphical representations in the form of scatter plots were produced. Each production day yielded 'billet' datasets that served as a foundation for initial data analysis; these datasets were subsequently segmented according to specific requirements to ascertain optimal methods for information integration—retaining only partitioning criteria that resulted in significant improvements in indices. These established partitions enabled work datasets necessary for assessing plant configuration alongside mathematical models (refer to Section 2.5).

To establish clusters based solely on billets processed within identical conditions—same production date, geometry, and similar furnace inlet temperatures (e.g., categorized as hot or cold)—the following partitioning criteria apply:

- Billets manufactured on identical production days;
- Group classification of reheated billets (1 through 4), with group 4 exclusively associated with billets measuring 0.14 m × 0.14 m;
- Thermal Imaging Camera Temperature Ranges: Data sets derived from thermal imaging camera measurements created homogeneous groups concerning outlet temperatures at the furnace;
- Diameter of finished products;
- Steel quality: This criterion further sub-divided previous classifications related to diameter into distinct categories based upon steel quality.

Characters within these clusters can represent billets sharing both quality attributes and diameters alike. For every operational day assessed under thermal imaging camera temperature range parameters, average values along with standard deviations from those readings led to defining seven distinct classes.

In order to calculate determination indices and correlation coefficients relating temperature metrics against stand absorption figures, comprehensive instrumentation was considered including three types of temperature sensors—the thermal imaging camera along with pyrometers located at both rolling mills—and absorption measures taken from nine different stands labeled numerically (1–9) as illustrated in Figures 3 and 4 respectively. Given varying measurement samples available per sensor corresponding each tracked billet instance percentile-based algorithms played an essential role extracting singular "global" values representing individual sensors across all tracked groups.

Figures such as Figures 6 and 7 depict typical trends observed via measurements gathered from respective sensors motivating development procedures aimed toward achieving unified "global" sensor value outcomes applicable across monitored billeted batches overall characterized visually where red indicates readouts obtained via thermal cameras while blue represents primary mill pyrometer results alongside green indicating secondary mill assessments highlighted throughout Figure 6's presentation showing how heat levels diminish during passage through rolling mill stages. Figure 7 illustrates current absorptions noted among various milling stands identified through color-coded signals marking processes initiated primarily by Stands one followed closely thereafter by Stand two represented using light blue/orange lines accordingly before progressing onward towards Stand three depicted herein yellow signal observations wherein additional five subsequent stages are addressed post intervals defined according aforementioned arrangements demonstrated prominently via referenced diagrams throughout Figures…

ISSN No:-2456-2165 https://doi.org/10.38124/ijisrt/25apr652

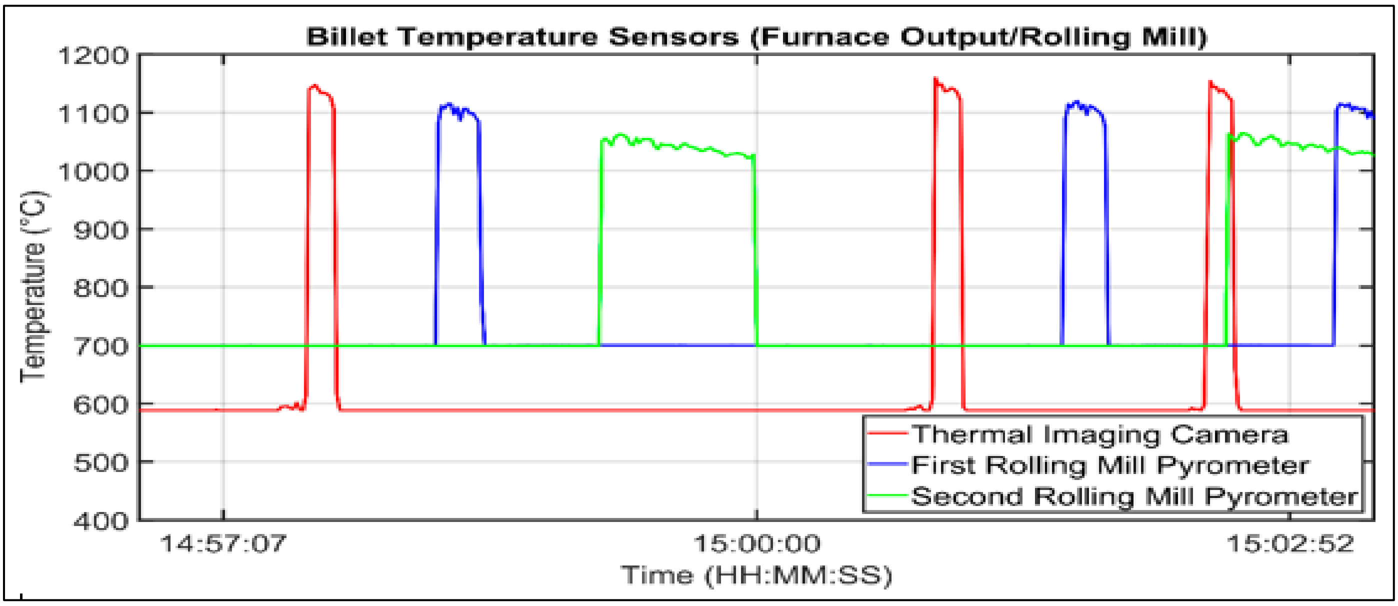

Fig 6 Billet Temperature sensors Measurements (furnace output/rolling mill).

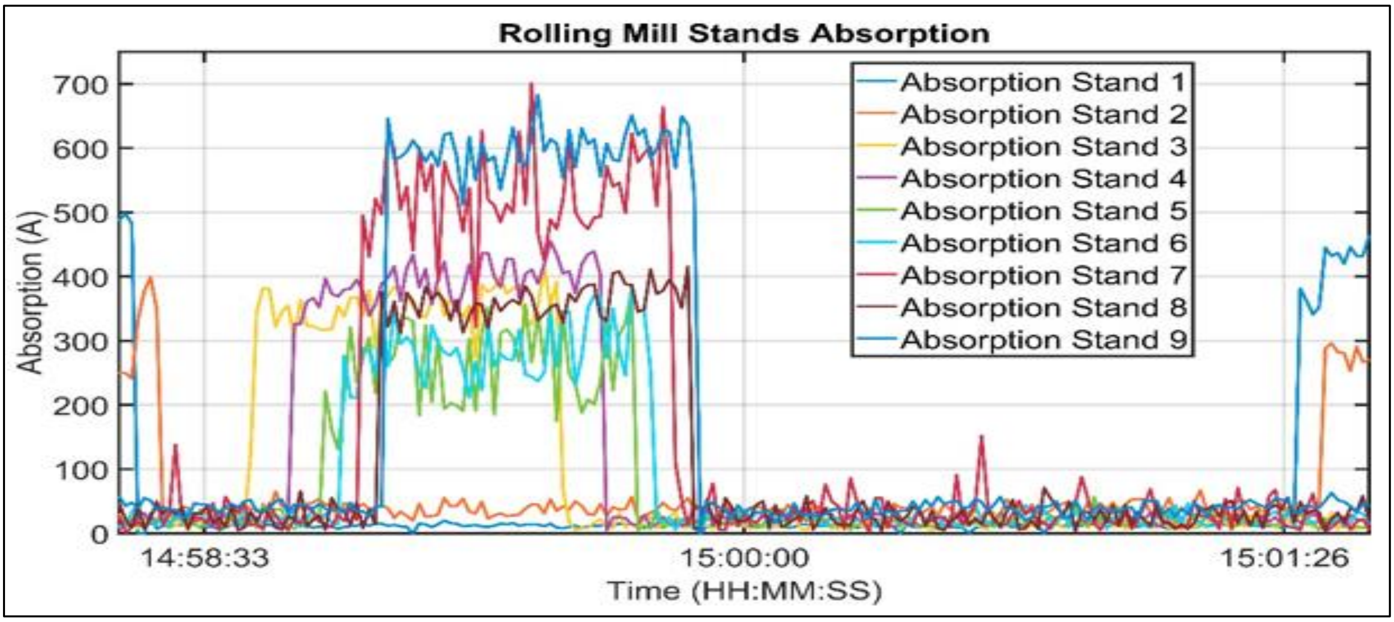

Fig 7 Rolling mill stands' Absorption Measurements.

E. Rolling Mill Stands' Billet Temperature Decay Mathematical Modelization

The model for temperature decay of billets in the rolling mill stands takes into account environmental factors from the exit of the furnace to the end of the stand area. The entry and exit points are identified through thermal imaging cameras and a pyrometer located downstream of stand 9. It is important to note that this analyzed route may differ based on specific plant configurations (as illustrated in Figures 3 and 4). This particular model relies on heat transfer equations ([1,28]) along with a segmentation strategy for tracking billet movement outside of the reheating furnace, tailored to each plant's setup. Following the original design layout (shown in Figures 3 and 8), it was proposed to divide billets' passage through the reheating process into six distinct stages.

- Thermal imaging camera-descaler movement;
- Descaler processing;
- Descaler-stand 1 movement;
- Rolling mill stand 1–2 processing;
- Stand 2-stand 3 movement;
- Stand 3-stand 9 processing.

ISSN No:-2456-2165 https://doi.org/10.38124/ijisrt/25apr652

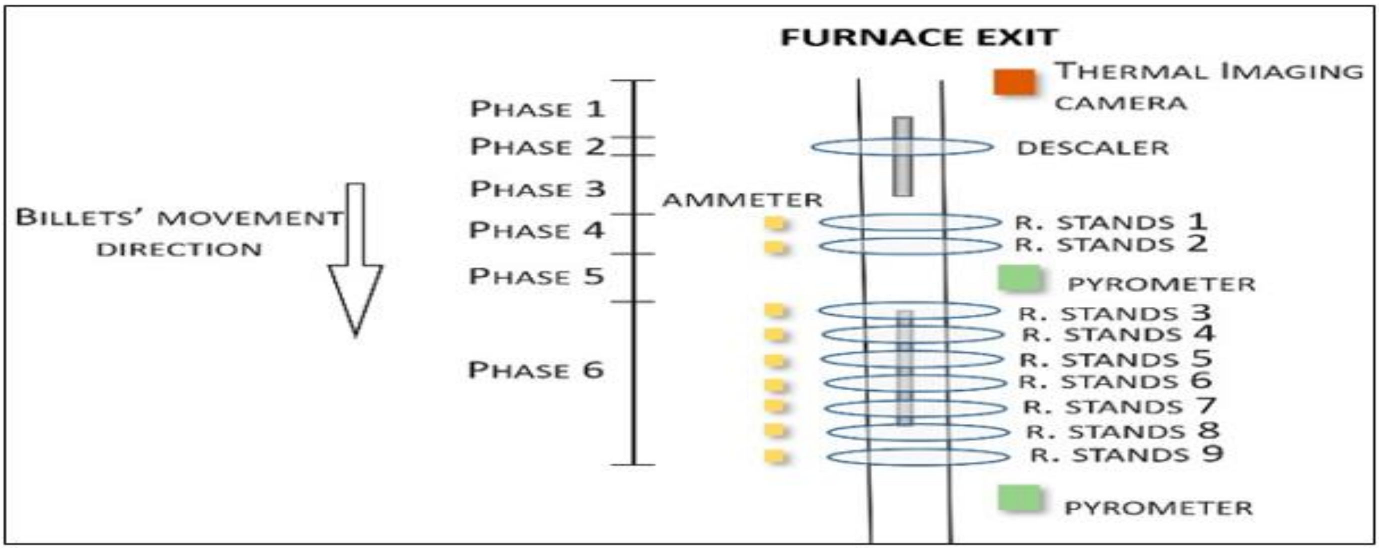

Fig 8 Original Configuration of the plant (including details on the Rolling mill Phase).

The phases associated with the initial configuration of the plant are illustrated in Figure 8. The model's starting conditions were established using measurements obtained from a thermal imaging camera. As depicted in Figure 8, this thermal imaging device is positioned upstream of phase 1 and provides temperature readings at the conclusion of the complete rolling mill process; specifically, it measures temperatures just prior to where a pyrometer installed downstream of phase 6 operates. To validate the model, these derived estimates were compared against this measured temperature.

Given these requirements, the purpose of the model was to forecast values recorded by a pyrometer placed downstream from stand 9 based on temperatures captured by a thermal imaging camera located at the furnace outlet—essentially upstream within overall processing considerations. A three-dimensional (3D) model was constructed for all monitored billets. Each tracked billet required its unique thermal model which utilized an initial singular thermal framework integrated with time evolution factors.

In developing this simulation, we incorporated essential elements such as Stefan–Boltzmann constant along with mesh and thermodynamic characteristics. Furthermore, scale formation modeling was included to accurately assess values related to thermal conductivity for each billet's upper layer since scales accumulate on surfaces during phases 1 and 2 [35,36].

To facilitate accurate simulations within our developed models regarding unknown parameters—crucial for computing heat transfer coefficients and assessing heat flow—we implemented various variables including: feed speed of billets; roll rotation speed; water temperature used during scale removal; transport roller temperatures; final thickness achieved after two rolling stages; roller-related parameters like work-hardening exponent and friction coefficient as well as radius proportions impacting rollers' resistance qualities—all alongside duration metrics across individual phases.

Billet attributes relevant here have been cataloged within Section 2.2 data frameworks . In order to evaluate how well our designed temperature decay model performed relative to actual results observed per examined billet—a percentage relative error metric has subsequently been calculated accordingly:

$$Error = \frac{T_{est} - T_{real}}{T_{real}} \cdot 100 \quad (1)$$

Treal represents the scalar value linked to the set of measurements obtained from the pyrometer located at stand 9 of the second rolling mill. Meanwhile, Test denotes the temperature prediction provided by the model for that specific location. Test corresponds to the average temperature noted upon completion of processing through the rolling mill, measured on top of the modeled billet, under the assumption that there is no consideration given in the 3D model regarding any reduction in thickness of the semi-finished product.

F. Computational Framework

The processing, analysis, and modeling of the temperature decay in rolling mill stands has been carried out within a MATLAB environment [37]. Functions available in MATLAB pertaining to scatter plots, determination indices, and correlation coefficient calculations were utilized for data preprocessing and analysis. The modeling was accomplished using the Partial Differential Equation Toolbox provided by MATLAB [37]. Specifically, this toolbox was primarily applied to the Heat Transfer feature which offered functions necessary for solving heat transfer equations as well as partial differential equations (PDE) through finite element methods. This work was executed on a laptop equipped with an Intel(R) Core(TM) i8-3840QM CPU running at 3.00GHz HDD capabilities up until 2023.

III. RESULTS AND DISCUSSION

This section presents the findings and discussions pertaining to the analysis of billet data as well as the mathematical modeling of temperature decay in rolling mill

ISSN No:-2456-2165 https://doi.org/10.38124/ijisrt/25apr652

stands. To summarize the results, we will use the following abbreviations: TIC for thermal imaging camera, FRMP for first rolling mill pyrometer, and SRMP for second rolling mill pyrometer.

A. Data Analysis Results (Original Plant Configuration)

Since the research outlined in section 2.4, the criteria employed for analyzing billet data resulted in distinct clusters based on factors such as production day, reheating group, thermal imaging camera temperature range, or product diameter. For billets produced on the same day, example values of determination indexes and correlation coefficients for each sensor are presented below in Table 4. The data displayed in Table 4 indicates that there is no significant correlation when using production day as a partitioning criterion.

- *This analysis was applied to all partition criteria mentioned earlier.*

Table 4 Data Analysis Results (*original* plant configuration) for the Billets with the same Production day.

Sensors	Determination Index	Correlation Coefficient
TIC–Stand 1 Abs.	0.1178	0.3432
TIC–Stand 2 Abs.	0.1031	0.3211
TIC–Stand 3 Abs.	0.0000045	0.0021
TIC–Stand 4 Abs.	0.0189	−0.1376
TIC–Stand 5 Abs.	0.0219	−0.1479
TIC–Stand 6 Abs.	0.0016	0.0397
TIC–Stand 7 Abs.	0.0038	−0.0616
TIC–Stand 8 Abs.	0.00028	0.0170
TIC–Stand 9 Abs.	0.0048	−0.0691
TIC–FRMP	0.0340	0.1844
TIC–SRMP	0.1942	0.4407
FRMP–SRMP	0.4627	0.6802
FRMP–Stand 1 Abs.	0.0877	−0.2961
FRMP–Stand 2 Abs.	0.0762	−0.2761
FRMP–Stand 3 Abs.	0.1055	−0.3249
FRMP–Stand 4 Abs.	0.0549	−0.2342
FRMP–Stand 5 Abs.	0.0381	−0.1953
FRMP–Stand 6 Abs.	0.0144	−0.1199
FRMP–Stand 7 Abs.	0.0364	−0.1908
FRMP–Stand 8 Abs.	0.0225	−0.1500
FRMP–Stand 9 Abs.	0.0211	−0.1453
SRMP–Stand 1 Abs.	0.000027	0.0052
SRMP–Stand 2 Abs.	0.00012	0.0109
SRMP–Stand 3 Abs.	0.0093	−0.0964
SRMP–Stand 4 Abs.	0.0159	−0.1262
SRMP–Stand 5 Abs.	0.0745	−0.2729
SRMP–Stand 6 Abs.	0.000012	−0.0035
SRMP–Stand 7 Abs.	0.0203	−0.1424
SRMP–Stand 8 Abs.	0.0019	−0.0441
SRMP–Stand 9 Abs.	0.0032	−0.0563

However, for most of the diameter groups examined, the pyrometers in the rolling mill exhibited superior correlation properties regarding current absorption by the rolling mill stands when compared to measurements taken with thermal imaging cameras. This finding indicates that the positioning of the rolling mill pyrometers relative to that of the thermal imaging camera (in actual plant settings) is more consistent. As a result, previously established criteria were discarded due to their lackluster performance. Implementing a fifth criterion produced favorable outcomes; consequently, we refined our previous criterion concerning finished product diameters into sub-clusters based on steel quality classifications. These clusters consist of billets sharing similar qualities and diameters. In Table 5, we present example values for determination indexes and correlation coefficients associated with each sensor considered.

Table 5 Data analysis results (*original* plant configuration) for the billets of the same steel quality and of the same diameter for the related finished products.

Sensors	Determination Index	Correlation Coefficient
TIC–Stand 1 Abs.	0.4007	−0.6330
TIC–Stand 2 Abs.	0.4840	−0.6957
TIC–Stand 3 Abs.	0.7240	−0.8509

ISSN No:-2456-2165 https://doi.org/10.38124/ijisrt/25apr652

TIC–Stand 4 Abs.	0.4953	−0.7038
TIC–Stand 5 Abs.	0.5532	−0.7438
TIC–Stand 6 Abs.	0.5176	−0.7195
TIC–Stand 7 Abs.	0.6279	−0.7924
TIC–Stand 8 Abs.	0.5799	−0.7615
TIC–Stand 9 Abs.	0.5636	−0.7507
TIC–FRMP	0.6017	0.7757
TIC–SRMP	0.6034	0.7768
FRMP–SRMP	0.8385	0.9157
FRMP–Stand 1 Abs.	0.4752	−0.6893
FRMP–Stand 2 Abs.	0.6633	−0.8144
FRMP–Stand 3 Abs.	0.8213	−0.9063
FRMP–Stand 4 Abs.	0.6740	−0.8209
FRMP–Stand 5 Abs.	0.7266	−0.8524
FRMP–Stand 6 Abs.	0.6043	−0.7773
FRMP–Stand 7 Abs.	0.6763	−0.8223
FRMP–Stand 8 Abs.	0.8218	−0.9066
FRMP–Stand 9 Abs.	0.7673	−0.8759
SRMP–Stand 1 Abs.	0.4308	−0.6564
SRMP–Stand 2 Abs.	0.6360	−0.7975
SRMP–Stand 3 Abs.	0.7936	−0.8908
SRMP–Stand 4 Abs.	0.7340	−0.8567
SRMP–Stand 5 Abs.	0.6775	−0.8231
SRMP–Stand 6 Abs.	0.6291	−0.7932
SRMP–Stand 7 Abs.	0.7094	−0.8423
SRMP–Stand 8 Abs.	0.7775	−0.8818
SRMP–Stand 9 Abs.	0.7994	−0.8941

Notice that upon examining Table 5, there is a noticeable enhancement in both the determination index and the correlation coefficient. This improvement has been observed across all generated groups according to the specified partition criterion; however, these results apply to all sensors except those paired with the thermal imaging camera. In general, this particular sensor exhibits poor correlation characteristics. For example, when it is placed at the outlet of the furnace or upstream of the descaler device, its readings may be affected by scale buildup on the billets.

Figures 9 and 10 display scatter plots corresponding to measurements from stand 9 as well as pyrometers from both rolling mills one and two. Additionally, an inverse relationship can be identified between absorption recorded in stand 9 and readings from both rolling mill pyrometers. This phenomenon can be attributed to lower temperature billets requiring greater force (and consequently higher current absorption) within a rolling mill stand for effective plastic deformation. Thus, these findings align with established physical principles governing the process under consideration.

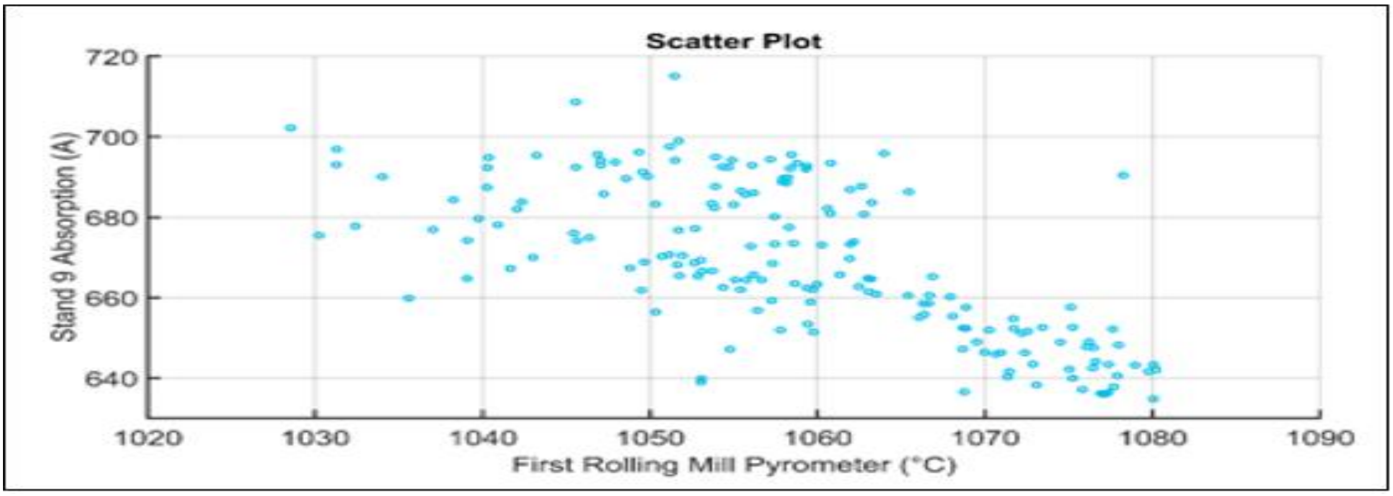

Fig 9 Scatter plot comparing the first rolling mill pyrometer and the absorption in stand 9.

ISSN No:-2456-2165 https://doi.org/10.38124/ijisrt/25apr652

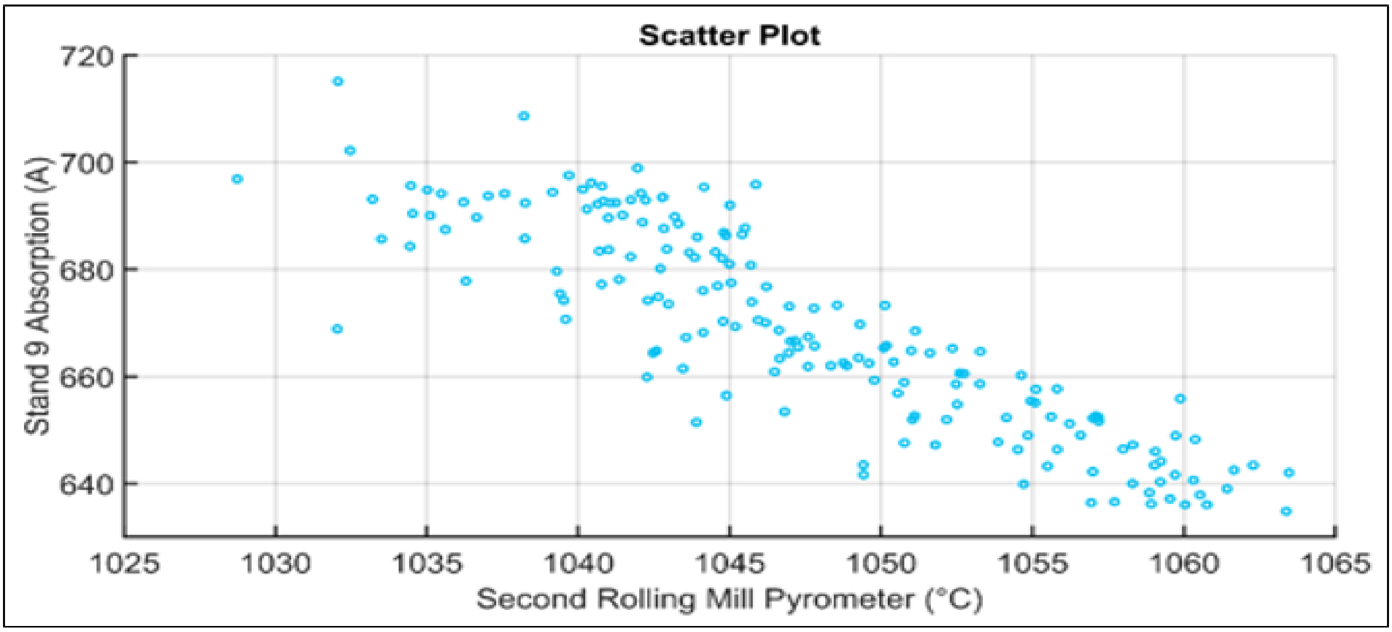

Fig 10 Scatter plot comparing the second rolling mill pyrometer and the absorption in stand 9.

B. Data Analysis Results (Modified Plant Configuration)

Results and discussions presented in Section 3.1 prompted a revision of the thermal imaging camera's placement to improve the reliability of its data. Figure 4 illustrates the updated configuration of the plant. It is important to note that in contrast to the original setup shown in Figures 3 and 8, the thermal imager has been relocated beyond the descaler area to mitigate any adverse effects caused by scale formation on its readings. With this new positioning for the thermal imaging camera, similar measures have been undertaken as outlined in Sections 2.2–2.4 (including adjustments made to the billet tracking system). The production days are now represented differently due to employing clustering methods discussed in Section 3.1.

The determination indexes and correlation coefficients pertaining to each example considered (billets sharing identical steel quality and corresponding finished product diameters) regarding both the thermal imaging camera and pyrometer from rolling mill two can be found in Table 6. As depicted in Figure 11, which features a scatter plot using two examples referenced from Table 6, there is an observable linear trend consistent with expectations. Table 7 offers an analysis akin to that provided in Table 6; however, it includes instances where certain clusters have been combined.

Table 6 Data analysis results (*modified* plant configuration) for the billets of the same steel quality and of the same diameter for the related finished products.

Sensors	**Determination Index**	**Correlation Coefficient**
TIC–SRMP (example 1)	0.896	0.9466
TIC–SRMP (example 2)	0.84	0.9165
TIC–SRMP (example 3)	0.75	0.8662
TIC–SRMP (example 4)	0.544	0.7376
TIC–SRMP (example 5)	0.5	0.7071
TIC–SRMP (example 6)	0.914	0.9560
TIC–SRMP (example 7)	0.773	0.8791
TIC–SRMP (example 8)	0.604	0.7771
TIC–SRMP (example 9)	0.542	0.7360

 International Journal of Innovative Science and Research Technology
ISSN No:-2456-2165 https://doi.org/10.38124/ijisrt/25apr652

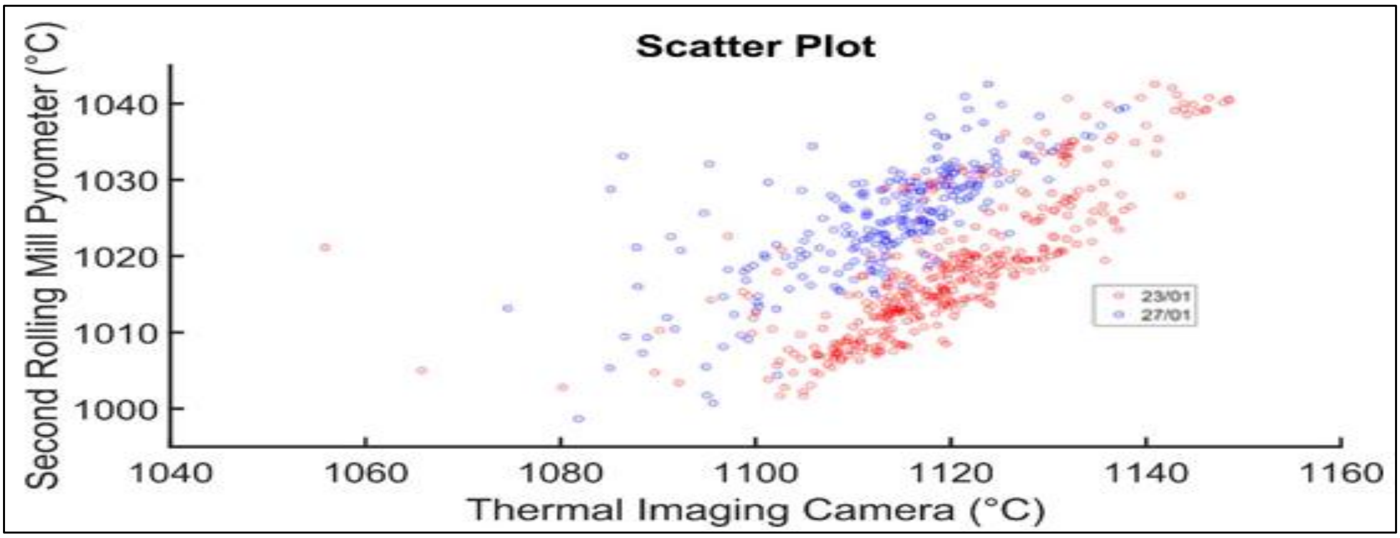

Fig 11 Scatter plot Comparing the thermal Imaging Camera and the second rolling mill Pyrometer.

Table 7 Data analysis results (*modified* plant configuration) for the billets of different clusters of steel quality and of the same diameter for the related finished products.

Sensors	Determination Index	Correlation Coefficient
TIC–SRMP (example 10)	0.616	0.7850
TIC–SRMP (example 11)	0.496	0.7042
TIC–SRMP (example 12)	0.267	0.5164
TIC–SRMP (example 13)	0.355	0.5956

The findings illustrated in **Table 6** and **Figure 11** indicate that repositioning the thermal imaging camera has led to improved correlation and determination metrics for the pairing of the thermal imaging camera with the second rolling mill pyrometer. The most effective (and notably satisfactory) outcomes are achieved through the clustering approach discussed in **Section 3.1**, where each cluster is composed of billets sharing identical steel quality and processing conditions from the rolling mill, resulting in uniform diameters for finished products. However, when certain billet clusters are combined, there is a decline in correlation characteristics (refer to **Table 7**). From a process perspective, this can be explained by differing physical properties among billets subjected to various treatments within the rolling mill. Consequently, constructing measurements from billets across multiple production clusters leads to uncorrelated data between the two sensors.

C. Modelization Results

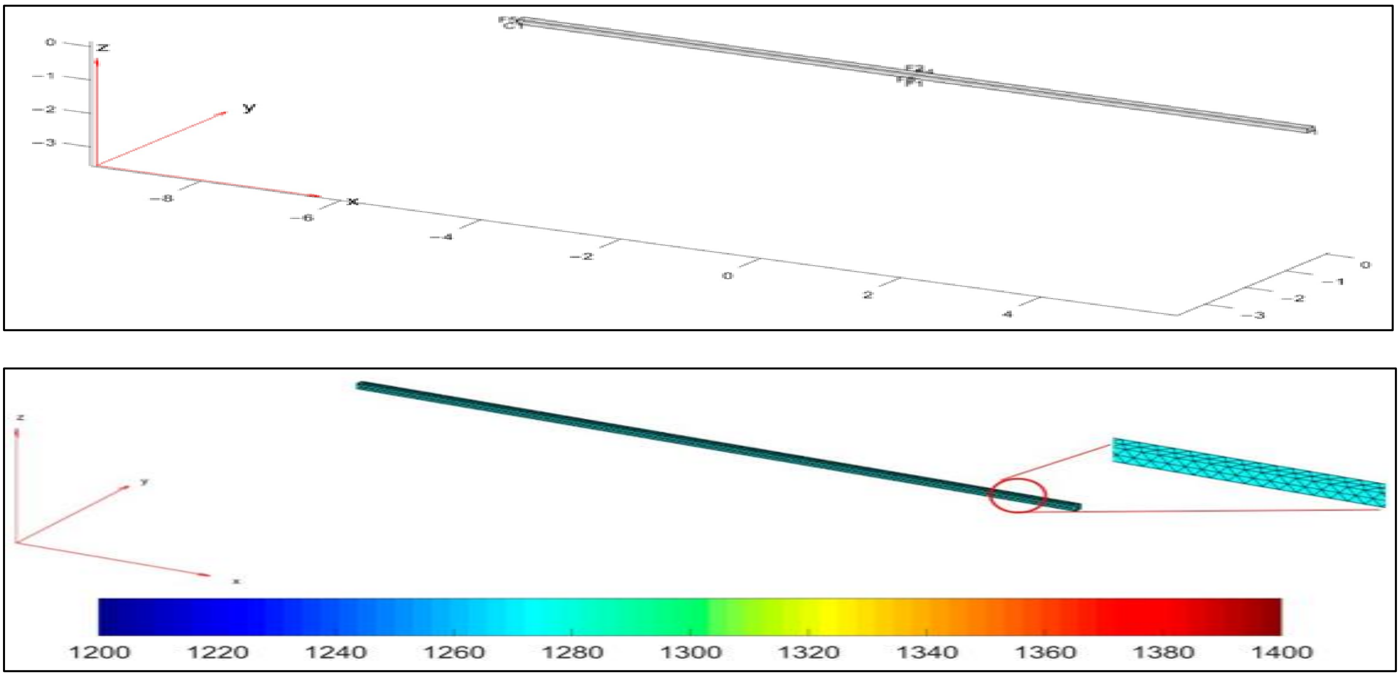

Fig 12 Modelization: 3D model of a billet, 3D model mesh, and color temperature scaling (K).

ISSN No:-2456-2165 https://doi.org/10.38124/ijisrt/25apr652

The mathematical modeling of temperature decline in billets within the rolling mill stands was constructed using a three-dimensional representation of the billets, incorporating specific meshing techniques and suitable color temperature scaling. This model also considers the initial layout of the plant. These features are illustrated in Figure 12.

Figures 13–18 present the simulation outcomes corresponding to each of the six stages of the modeling process (temperature is measured in Kelvin, and time is recorded in seconds). The concluding state of one phase serves as the starting point for the next. This simulation pertains to a billet with these specific characteristics:

- Length: 11.9 m;
- Section: 0.14 m × 0.14 m;
- Mass: 1830 kg;
- Rolling mill ambient temperature: 18.9 °C;
- Thermal camera temperature: 1108 °C;
- Rolling mill phase duration: 89.911 s;
- Second rolling pyrometer temperature: 1034 °C.

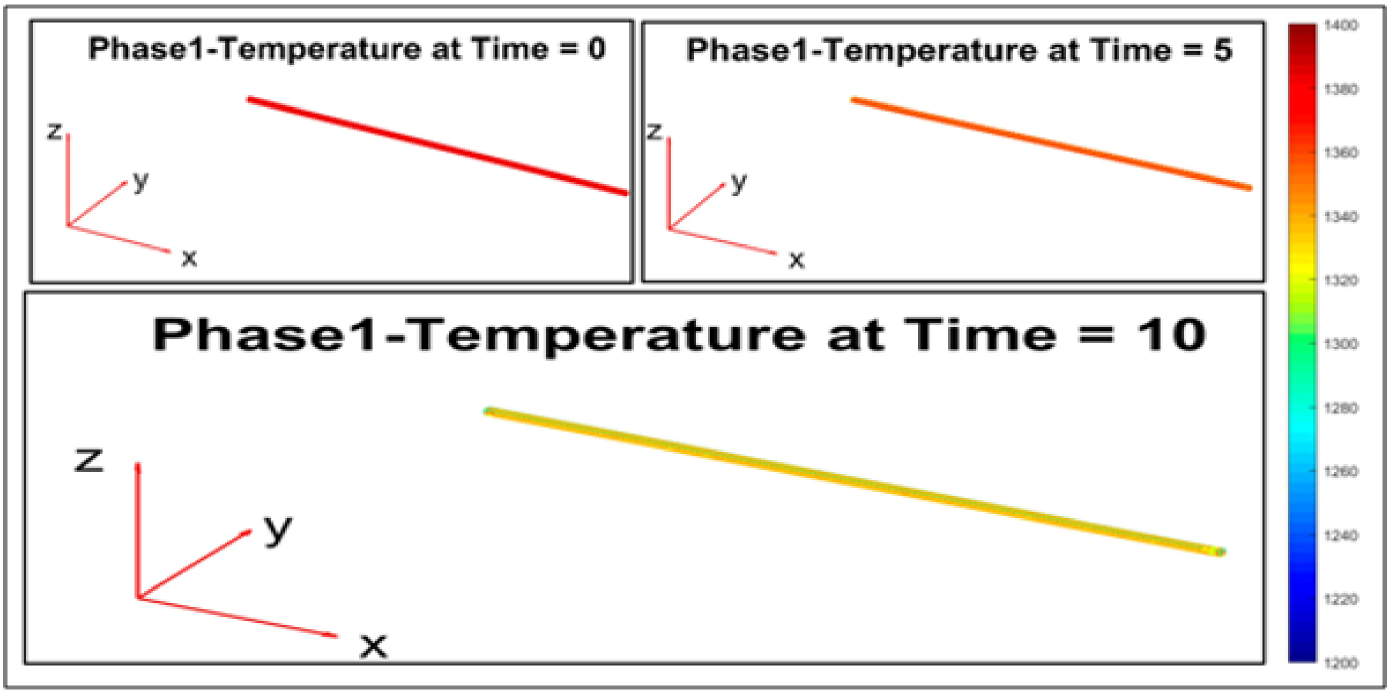

Fig 13 Modelization: phase 1 (Movement between the Thermal Imaging Camera and the Descaler).

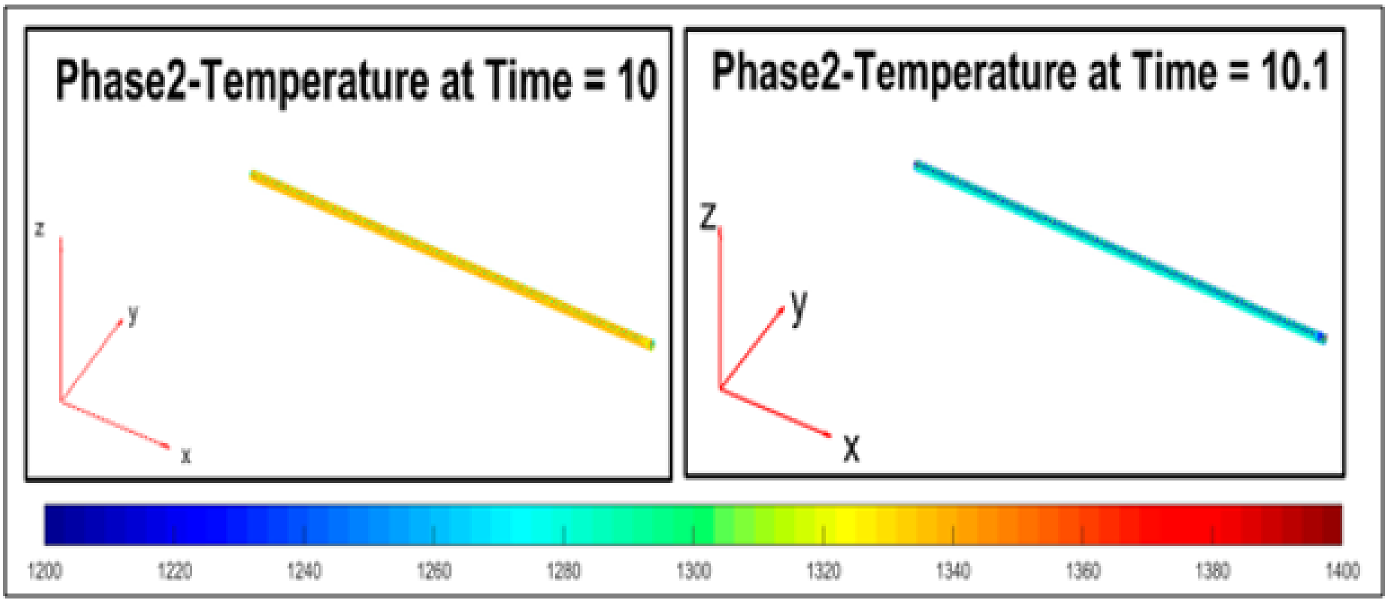

Fig 14 Modelization: phase 2 (Descaler Processing).

ISSN No:-2456-2165 https://doi.org/10.38124/ijisrt/25apr652

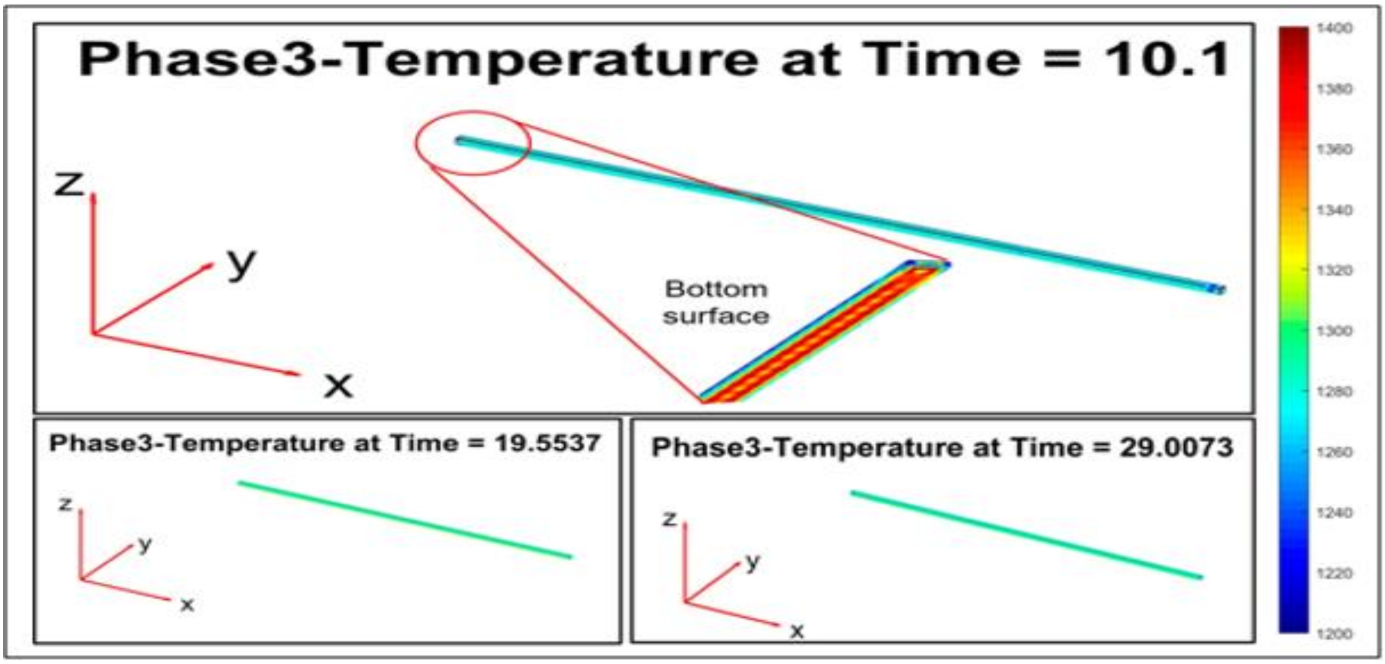

Fig 15 Modelization: phase 3 (Movement between the Descaler and Stand 1).

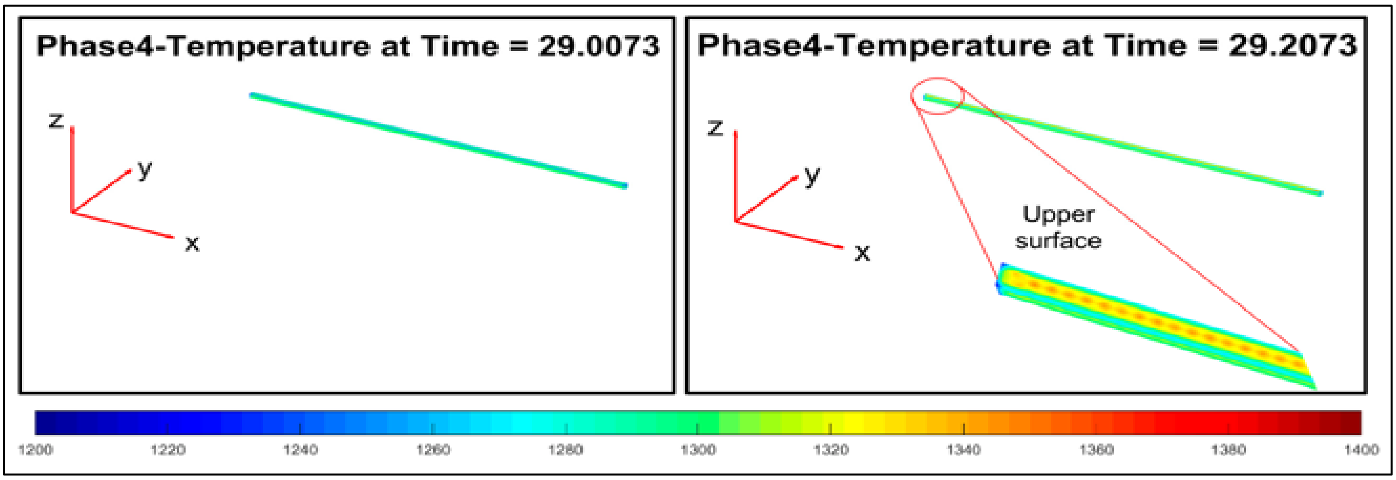

Fig 16 Modelization: phase 4 (processing between rolling mill stands 1–2).

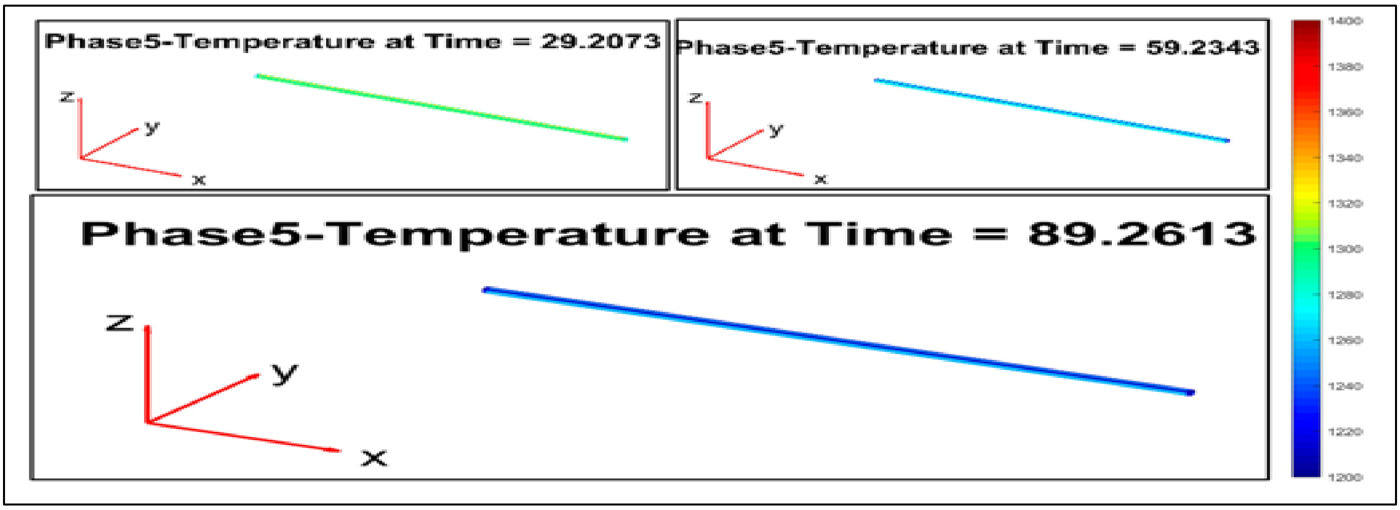

Fig 17 Modelization: phase 5 (movement between stand 2 and stand 3).

ISSN No:-2456-2165 https://doi.org/10.38124/ijisrt/25apr652

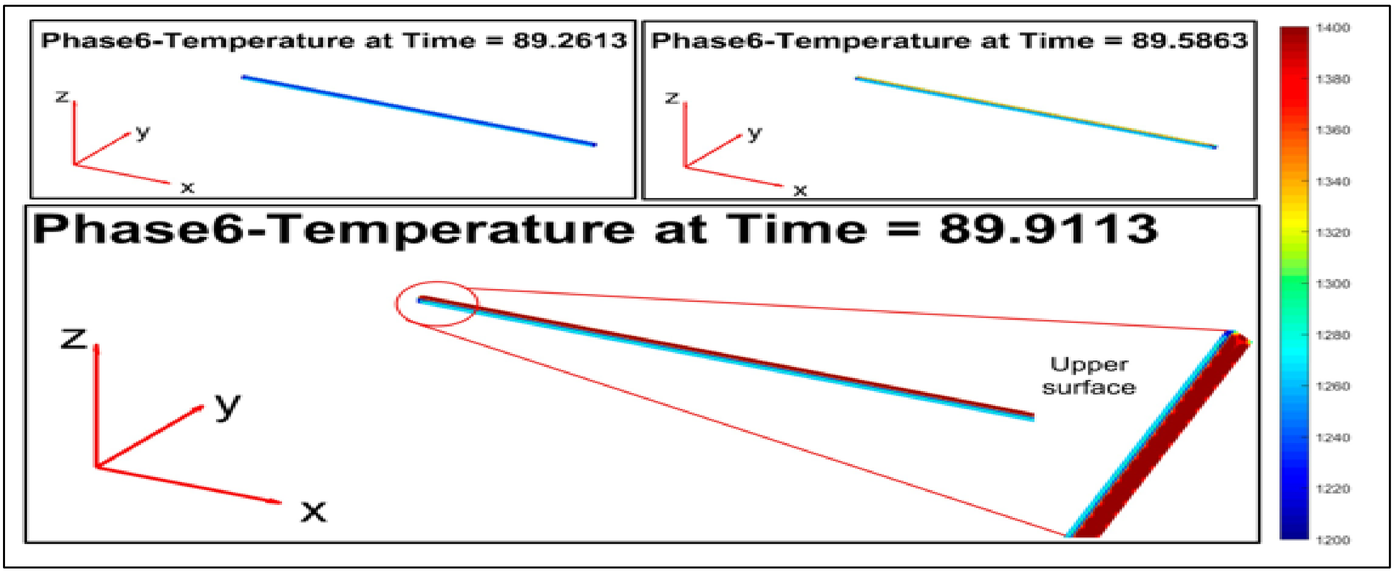

Fig 18 Modelization: phase 6 (processing between stand 3 and stand 9).

These data pertain to a billet that traversed the designated tracking system. As illustrated in the initial stage (Figure 13), it is evident that the temperature of the billet layers diminishes due to heat transfer phenomena, including radiation and natural convection with surrounding air. The lower layer's temperature remains elevated compared to other layers because of heat generated by transport rollers. In the second phase (Figure 14), forced convection occurs between the billet and water jets from a descaling device, facilitating scale removal primarily on top and side surfaces. This focus for simulation is warranted since direct contact between transport rollers and bottom layers suggests minimal scale formation there.

During Phase 3 (Figure 15), temperatures among varying billets levels equalize as upward heat flow increases temperatures at both upper surfaces and sides while subsequently causing a reduction through radiation and natural convection interactions with ambient air. Due to ongoing heat generation from transport rollers, it can be expected that lower layer temperatures will remain higher than those above.

The gradual warming effect observed on the uppermost layer during strong friction simulations involving rolling mill stands becomes apparent in this phase (Phase 4, Figure 16). Phase 5 mirrors Phase 1 as another decrease in billet temperature continues; Step Six (Figure18) aligns with Step Four where significant friction from the second rolling mill stand raises temperatures within upper microscopic layers of steel.

At simulation's conclusion, models predict an average top-layer temperature reaching **1042°C**, contrasting slightly against actual measured values at **1034°C**, yielding a relative error rate calculated via Equation (1) amounting to **0.773%**.In section ***3.1*** concerning data analysis across complete datasets proved essential for establishing an accurate representative subset necessary for model evaluation; consequently eliminating clusters exhibiting weak correlation-determination results was imperative.

IV. CONCLUSIONS

This research was conducted to address specific aspects of data analysis and modeling within the steel industry, focusing particularly on the billet preheating phase and the overall rolling mill area. Initially, a comprehensive assessment was carried out using measurements from billet temperature sensors (including thermal imaging cameras and pyrometers in the rolling mills) alongside current absorption values observed in various stands of the mill. This evaluation led to identifying that for achieving adequate correlation results, it is essential to categorize billets according to their respective steel types and final product specifications.

The importance of data analysis became evident when determining a relevant subset characterized by stable correlation indices suitable for model evaluation. Utilizing properties derived from clusters of billets with sufficient correlation attributes, a mathematical model representing temperature decay was formulated; this model correlated with the trajectories taken by billets as they exited the reheating furnace.

The surface temperatures recorded on these billets—closely tied to how heat transfer behaves dynamically—were significantly influenced by several factors including varying initial temperatures during processing phases, potential halts throughout those phases, along with geometric and physical characteristics inherent in each billet. All these variables were accounted for while calibrating the developed temperature decay model resulting in relatively low percentage errors associated with modeling accuracy.

Moreover, analyzed data indicated that scale formation has considerable implications on measurements obtained via thermal imaging cameras. To enhance correlation metrics between readings from thermal imaging devices and rolling mill pyrometers further improvements were made: positioning thermal cameras after descaling equipment downstream from subsequent stands within milling operations.

Future endeavors will focus on modeling how temperature evolves across billets during their passage through production mills utilizing updated information reflecting changes regarding camera placement. Additionally, more thorough analyses concerning individual reheating conditions experienced by each billet inside furnaces could be beneficially explored. Furthermore, implementing adjustments based upon recent sensor configurations combined with proposed methodologies can aid effectively managing constraints pertinent to an advanced process control system grounded in predictive control strategies [1].

REFERENCES

[1]. Zanoli, S.M.; Cocchioni, F.; Pepe, C. MPC-based energy efficiency improvement in a pusher type billets reheating furnace. Adv. Sci. Technol. Eng. Syst. J. 2018, 3, 74–84. [CrossRef]

[2]. Zanoli, S.M.; Orlietti, L.; Cocchioni, F.; Astolfi, G.; Pepe, C. Optimization of the clinker production phase in a cement plant. In CONTROLO 2020. Lecture Notes in Electrical Engineering; Gonçalves, J.A., Braz-César, M., Coelho, J.P., Eds.; Springer: Cham, Switzerland, 2021; Volume 695. [CrossRef]

[3]. Borel-Saladin, J.M.; Turok, I.N. The Green Economy: Incremental Change or Transformation? Environ. Policy Gov. 2013, 23, 209–220. [CrossRef]

[4]. Agenda 2030. Available online: https://unric.org/it/agenda-2030/ (accessed on 11 August 2022).

[5]. PNRR. Available online: https://www.mise.gov.it/index.php/it/pnrr (accessed on 11 August 2022).

[6]. Cavaliere, P. Clean Ironmaking and Steelmaking Processes: Efficient Technologies for Greenhouse Emissions Abatement; Springer: Cham, Switzerland, 2019. [CrossRef]

[7]. Holappa, L. Challenges and Prospects of Steelmaking towards the Year 2050. Metals 2021, 11, 1978. [CrossRef]

[8]. Wu, M.; Cao, W.; Chen, X.; She, J. Intelligent Optimization and Control of Complex Metallurgical Processes; Springer: Singapore, 2020. [CrossRef]

[9]. Steinbock, A. Model-Based Control and Optimization of a Continuous Slab Reheating Furnace; Shaker: Düren, Germany, 2011.

[10]. Bonci, A.; Pirani, M.; Longhi, S. A DataBase-Centric Framework for the Modeling, Simulation, and Control of Cyber-Physical Systems in the Factory of the Future. J. Intell. Syst. 2018, 27, 659–679. [CrossRef]

[11]. Trinks, W.; Mawhinney, M.H.; Shannon, R.A.; Reed, R.J.; Garvey, J.R. Industrial Furnaces; John Wiley & Sons: New York, NY, USA, 2004. [CrossRef]

[12]. Mullinger, P.; Jenkins, B. Industrial and Process Furnaces.Principles, Design and Operation; Elsevier: Amsterdam, The Netherlands, 2008. [CrossRef]

[13]. Zhang, Y.; Li, Q.; Zhou, H. Theory and Calculation of Heat Transfer in Furnaces; Elsevier: Amsterdam, The Netherlands, 2016.

[14]. NIIR Board of Consultants & Engineers. Steel Rolling Technology Handbook; Asia Pacific Business Press Inc.: New Delhi, India, 2018.

[15]. NIIR Board of Consultants & Engineers. The Complete Technology Book on Hot Rolling of Steel; Niir Project Consultancy Services: New Delhi, India, 2010.

[16]. NIIR Board of Consultants & Engineers. The Complete Technology Book on Steel and Steel Products; Asia Pacific Business Press Inc.: New Delhi, India, 2008.

[17]. Mui, C. Steel BilletReheating: An Expert Approach. Master of Applied Science. Ph.D. Thesis, The University of British Columbia, Vancouver, BC, Canada, 15 October 1998.

[18]. Development of Next Generation Heating System for Scale Free Steel Reheating. Available online: https://www.osti.gov/ servlets/purl/1004059 (accessed on 11 August 2022).

[19]. Sarda, K.; Yerudkar, A.; Vecchio, C.D. Missing data imputation for real time-SERIES data in a steel industry using generative adversarial networks. In Proceedings of the IECON 2021—47th Annual Conference of the IEEE Industrial Electronics Society, Toronto, ON, Canada, 13–16 October 2021. [CrossRef]

[20]. Wu, H.; Jin, F.; Zhao, J.; Wang, W. Anomaly detection method based on multi-criteria evaluation for energy data of steel industry. In Proceedings of the 2021 IEEE 10th Data Driven Control and Learning Systems Conference (DDCLS), Suzhou, China, 14–16 May 2021. [CrossRef]

[21]. Zhang, L.; Zou, D. Product quality prediction of rolling mill in big data environment. In Proceedings of the 2020 International Conference on Big Data and Informatization Education (ICBDIE), Zhangjiajie, China, 23–25 April 2020. [CrossRef]

[22]. Hsu, C.-Y.; Kang, L.-W.; Lin, H.-Y.; Fu, R.-H.; Lin, C.-Y.; Weng, M.-F.; Chen, D.-Y. Depth-based feature extraction-guided automatic identification tracking of steel products for smart manufacturing in steel 4.0. In Proceedings of the 2018 IEEE International Conference on Applied System Invention (ICASI), Chiba, Japan, 13–17 April 2018. [CrossRef]

[23]. Zhukov, P.; Fomin, A.; Glushchenko, A. Development of Relationship Between Steel Billet Temperature and Data on Its Heating History for Continuous Furnace of Rolling-Mill Shop. In Proceedings of the 2020 2nd International Conference on Control Systems, Mathematical Modeling, Automation and Energy Efficiency (SUMMA), Lipetsk, Russia, 11–13 November 2020. [CrossRef]

ISSN No:-2456-2165 https://doi.org/10.38124/ijisrt/25apr652

[24]. Xu, Z.; Hua, T.; Fan, X.; Zhu, X. Research on the Strategy of Delay Rolling for Reheating Furnace based on Swarm Intelligence Algorithm. In Proceedings of the 2022 7th International Conference on Intelligent Computing and Signal Processing (ICSP), Xi'an, China, 15–17 April 2022. [CrossRef]

[25]. Chen, C.-J.; Chou, F.-I.; Chou, J.-H. Temperature Prediction for Reheating Furnace by Gated Recurrent Unit Approach. IEEE Access 2022, 10, 33362–33369. [CrossRef]

[26]. Zhukov, P.; Fomin, A.; Glushchenko, A.; Podvalnyi, E. Comparison of finite-difference and data-based models of temperature transfer process in heating furnaces for cast billet temperature prediction. In Proceedings of the 2020 2nd International Con- ference on Control Systems, Mathematical Modeling, Automation and Energy Efficiency (SUMMA), Lipetsk, Russia, 10–12 November 2021. [CrossRef]

[27]. Zanoli, S.M.; Pepe, C.; Astolfi, G.; Moscoloni, E. Analysis and modeling of steel industry reheating furnace billets temperature. In Proceedings of the 2022 23rd International Carpathian Control Conference (ICCC), Sinaia, Romania, 29 May–1 June 2022; pp. 337–342. [CrossRef]

[28]. Moscoloni, E. Analisi e Modellazione Della Temperatura di Semilavorati di un Forno di Riscaldo di un'acciaieria. Master's Thesis, Università Politecnica delle Marche, Ancona, Italy, 2020. Supervisor: Zanoli, S.M..

[29]. Åström, K.J.; Hägglund, T. PID Controllers: Theory, Design, and Tuning; ISA—The Instrumentation, Systems and Automation Society: Research Triangle Park, NC, USA, 1995.

[30]. Borja-Castro, L.E.; Bustamante Dominguez, A.; Valerio-Cuadros, M.I.; Valencia-Bedregal, R.A.; Cabrera-Tinoco, H.A.; Espinoza Suarez, S.M.; Kargin, J.; Moreno, N.O.; Barnes, C.H.W.; De Los Santos Valladares, L. Characterization of steel billet scales generated during the continuous casting process in SIDERPERU steel plant. Hyperfine Interact. 2021, 242, 53. [CrossRef]

[31]. Wang, Z.-C.; Sun, X.-D.; Yuan, W. Influence of oxide scale on continuous casting billet on thickness measurement by electro- magnetic ultrasonic transducer. In Proceedings of the 2018 5th International Conference on Information Science and Control Engineering (ICISCE), Zhengzhou, China, 20–22 July 2018. [CrossRef]

[32]. Kelleher, J.D.; Tierney, B. Data Science; MIT Press: Cambridge, MA, USA, 2018.

[33]. Archdeacon, T. Correlation and Regression Analysis: A Historian's Guide; University of Wisconsin Press: Madison, WI, USA, 1994.

[34]. Navidi, W. Probabilità e Statistica per L'ingegneria e le Scienze; McGraw-Hill Education: New York, NY, USA, 2006.

[35]. Jaklicˇ, A.; Glogovac, B.; Kolenko, T.; Zupancˇicˇ, B.; Težak, B. A simulation of heat transfer during billet transport. Appl. Therm. Eng. 2002, 22, 873–883. [CrossRef]

[36]. Serajzadeh, S.; Mirbagheri, H.; Karimi Taheri, A. Modelling the temperature distribution and microstructural changes during hot rod rolling of a low carbon steel. J. Mater. Process. Technol. 2002, 125–126, 89–96. [CrossRef]

[37]. MathWorks. Available online: https://it.mathworks.com/ (accessed on 13 August 2022).